Synthesis of highly focused fields with circular polarization at any transverse plane

David Maluenda,[1] **Rosario Martínez-Herrero,** [2] **Ignasi Juvells,**[1] **and Artur Carnicer**[1,*]

[1]*Departament de Física Aplicada i Òptica, Universitat de Barcelona (UB), Martí i Franquès 1, 08028 Barcelona (Spain)*

[2]*Departamento de Óptica, Facultad de Ciencias Físicas, Universidad Complutense de Madrid, 28040 Madrid (Spain)*

[*]*artur.carnicer@ub.edu*

Abstract: We develop a method for generating focused vector beams with circular polarization at any transverse plane. Based on the Richards-Wolf vector model, we derive analytical expressions to describe the propagation of these set of beams near the focal area. Since the polarization and the amplitude of the input beam are not uniform, an interferometric system capable of generating spatially-variant polarized beams has to be used. In particular, this wavefront is manipulated by means of spatial light modulators displaying computer generated holograms and subsequently focused using a high numerical aperture objective lens. Experimental results using a $NA = 0.85$ system are provided: irradiance and Stokes images of the focused field at different planes near the focal plane are presented and compared with those obtained by numerical simulation.

OCIS codes: (260.5430) Polarization; (090.1760) Computer holography; (070.6120) Spatial light modulators.

References and links

1. R. Dorn, S. Quabis, and G. Leuchs, "Sharper focus for a radially polarized light beam," Phys. Rev, Lett. **91**, 233901 (2003).
2. N. Davidson and N. Bokor, "High-numerical-aperture focusing of radially polarized doughnut beams with a parabolic mirror and a flat diffractive lens," Opt. Lett. **29**, 1318–1320 (2004).
3. M. Leutenegger, R. Rao, R. A. Leitgeb, and T. Lasser, "Fast focus field calculations," Opt. Express **14**, 11277–11291 (2006).
4. Y. Kozawa and S. Sato, "Sharper focal spot formed by higher-order radially polarized laser beams," J. Opt. Soc. Am. A **24**, 1793–1798 (2007).
5. H. Wang, L. Shi, B. Lukyanchuk, C. Sheppard, and C. T. Chong, "Creation of a needle of longitudinally polarized light in vacuum using binary optics," Nature Photon. **2**, 501–505 (2008).
6. G. Lerman and U. Levy, "Effect of radial polarization and apodization on spot size under tight focusing conditions," Opt. Express **16**, 4567–4581 (2008).
7. X. Hao, C. Kuang, T. Wang, and X. Liu, "Phase encoding for sharper focus of the azimuthally polarized beam," Opt. Lett. **35**, 3928–3930 (2010).
8. S. N. Khonina and S. G. Volotovsky, "Controlling the contribution of the electric field components to the focus of a high-aperture lens using binary phase structures," J. Opt. Soc. Am. A **27**, 2188–2197 (2010).
9. Q. Zhan, "Cylindrical vector beams: from mathematical concepts to applications," Adv. Opt. Photon. **1**, 1–57 (2009).
10. R. Martınez-Herrero, I. Juvells, and A. Carnicer, "On the physical realizability of highly focused electromagnetic field distributions," Opt. Lett. **38**, 2065–2067 (2013).

11. M. R. Foreman, S. S. Sherif and P. R. T. Munro and P. Török, “Inversion of the Debye-Wolf diffraction integral using an eigenfunction representation of the electric fields in the focal region,” Opt. Express **16**, 4901–4917 (2008).
12. K. Jahn, and N. Bokor, “Solving the inverse problem of high numerical aperture focusing using vector Slepian harmonics and vector Slepian multipole fields”, Opt. Commun. **288**, 13–16 (2013).
13. C. Maurer, A. Jesacher, S. Fürhapter, S. Bernet, and M. Ritsch-Marte, “Tailoring of arbitrary optical vector beams,” New J. Phys. **9**, 78 (2007).
14. H.-T. Wang, X.-L. Wang, Y. Li, J. Chen, C.-S. Guo, and J. Ding, “A new type of vector fields with hybrid states of polarization,” Opt. Express **18**, 10786–10795 (2010).
15. I. Moreno, C. Iemmi, J. Campos, and M. Yzuel, “Jones matrix treatment for optical Fourier processors with structured polarization,” Opt. Express **19**, 4583–4594 (2011).
16. F. Kenny, D. Lara, O. G. Rodríguez-Herrera, and C. Dainty, “Complete polarization and phase control for focus-shaping in high-na microscopy,” Opt. Express **20**, 14015–14029 (2012).
17. D. Maluenda, I. Juvells, R. Martínez-Herrero, and A. Carnicer, “Reconfigurable beams with arbitrary polarization and shape distributions at a given plane,” Opt. Express **21**, 5432–5439 (2013).
18. W. Han, Y. Yang, W. Cheng, and Q. Zhan, “Vectorial optical field generator for the creation of arbitrarily complex fields,” Opt. Express **21**, 20692–20706 (2013).
19. E. H. Waller and G. von Freymann, “Independent spatial intensity, phase and polarization distributions,” Opt. Express **21**, 28167–28174 (2013).
20. Z.-Y. Rong, Y.-J. Han, S.-Z. Wang, and C.-S Guo, “Generation of arbitrary vector beams with cascaded liquid crystal spatial light modulators,” Opt. Express **22**, 1636–1644 (2014).
21. C.-S. Guo, Z.-Y. Rong, and S.-Z. Wang, “Double-channel vector spatial light modulator for generation of arbitrary complex vector beams,” Opt. Lett. **39**, 386–389 (2014).
22. G. Brakenhoff, P. Blom, and P. Barends, “Confocal scanning light microscopy with high aperture immersion lenses,” J. Microsc. **117**, 219–232 (1979).
23. C. Sheppard and A. Choudhury, “Annular pupils, radial polarization, and superresolution,” Appl. Opt. **43**, 4322–4327 (2004).
24. K. Kitamura, K. Sakai, and S. Noda, “Sub-wavelength focal spot with long depth of focus generated by radially polarized, narrow-width annular beam,” Opt. Express **18**, 4518–4525 (2010).
25. D. Biss and T. Brown, “Polarization-vortex-driven second-harmonic generation,” Opt. Lett. **28**, 923–925 (2003).
26. D. Oron, E. Tal, and Y. Silberberg, “Depth-resolved multiphoton polarization microscopy by third-harmonic generation,” Opt. Lett. **28**, 2315–2317 (2003).
27. O. Masihzadeh, P. Schlup, and R. A. Bartels, “Enhanced spatial resolution in third-harmonic microscopy through polarization switching,” Opt. Lett. **34**, 1240–1242 (2009).
28. Y. Gorodetski, A. Niv, V. Kleiner, and E. Hasman, “Observation of the spin-based plasmonic effect in nanoscale structures,” Phys. Rev. Lett. **101**, 043903 (2008).
29. L. Vuong, A. Adam, J. Brok, P. Planken, and H. Urbach, “Electromagnetic spin-orbit interactions via scattering of subwavelength apertures,” Phys. Rev. Lett. **104**, 083903 (2010).
30. L. D. Barron, *Molecular Light Scattering and Optical Activity* (Cambridge University, 2004).
31. Y. Inoue and V. Ramamurthy, *Chiral Photochemistry* (CRC, 2004).
32. A. Turpin, Y. V. Loiko, T. K. Kalkandjiev, and J. Mompart, “Multiple rings formation in cascaded conical refraction,” Opt. Lett. **38**, 1455–1457 (2013).
33. B. Richards and E. Wolf, “Electromagnetic diffraction in optical systems. II. Structure of the image field in an aplanatic system,” P. Roy. Soc. London A Mat. **253**, 358–379 (1959).
34. V. Arrizón, L. González, R. Ponce, and A. Serrano-Heredia, “Computer-generated holograms with optimum bandwidths obtained with twisted-nematic liquid-crystal displays,” Appl. Opt. **44**, 1625–1634 (2005).
35. V. Arrizón, “Complex modulation with a twisted-nematic liquid-crystal spatial light modulator: double-pixel approach,” Opt. Lett. **28**, 1359–1361 (2003).
36. M. Born and E. Wolf, *Principles of Optics: Electromagnetic Theory of Propagation, Interference and Diffraction of Light* (Cambridge University, 1999).

1. Introduction

The propagation of electromagnetic field distributions generated at the focal region has been extensively investigated in the last years [1–8]. Non-paraxial fields have demonstrated very useful in many fields for instance in high-resolution microscopy, particle trapping, high-density recording, tomography, electron acceleration, nonlinear optics, and optical tweezers [9]. Beam shaping in the focal area of a high numerical aperture objective lens requires a careful design of the input wavefront. In particular, full control of the complex amplitude and polarization distributions of the paraxial input field is required to generate focused fields adapted to the

#205396 - $15.00 USD Received 23 Jan 2014; revised 4 Mar 2014; accepted 5 Mar 2014; published 17 Mar 2014

requirements of a specific problem [10]. Interestingly, several authors described inverse methods to find the pupil function from a predetermined field distribution in the focal area [11, 12]. Light shaping can be accomplished by using an optical setup able to generate beams with arbitrary polarization and shape distributions at a given plane. This is usually carried out by means of interferometric systems in combination with spatial light modulators and digital holography [13–21]. The objective of this paper is to present a method for designing focused fields with transverse circular polarization at any plane. Among many others applications, circularly polarized tight focused beams are useful in resolution improvement [22–24], third harmonic generation-based microscopy [25–27], plasmonics and nano-optics applications [28, 29], optical activity and chemical related problems [30, 31] or, conical refraction [32].

Using the Richards-Wolf vector diffraction theory, we derive analytical expressions to describe the propagation of these set of beams near the focal area. Complex amplitude and polarization of the input beam are manipulated by means of spatial light modulators (SLM) displaying computer generated holograms. Numerical calculations and experimental results are compared and analyzed. Accordingly, the paper is organized as follows: in section 2 we derive the equations for describing circularly-polarized focused fields at any transverse plane. The experimental setup and the holographic procedure required to synthesize the beam are reviewed in section 3. Experimental results including irradiance images and polarization analysis are presented in section 4. Finally, the main conclusions are summarized in section 5.

2. Circularly-polarized highly focused beams

The electromagnetic field in the focal area of a high numerical aperture objective lens that obeys the sine condition is described by the Richards-Wolf vector equation [33]

$$\begin{aligned}\mathbf{E}(r,\phi,z) = A\int_0^{\theta_0}\int_0^{2\pi}&\sqrt{\cos\theta}\left[f_1(\theta,\varphi)\,\mathbf{e_1}(\varphi)+f_2(\theta,\varphi)\,\mathbf{e_2^o}(\theta,\varphi)\right]\\ &\times\, e^{ikr\sin\theta\cos(\phi-\varphi)}e^{-ikz\cos\theta}\sin\theta\,d\theta\,d\varphi\,,\end{aligned} \tag{1}$$

where A is a constant, r, ϕ and z are the coordinates in the focal area, and angles φ and θ are the coordinates at the exit pupil; note that θ_0 is the semi-aperture angle. Functions $f_1(\theta,\varphi)$ and $f_2(\theta,\varphi)$ are the azimuthal and radial components of incident field respectively,

$$f_1(\theta,\varphi) = \mathbf{E}_S(\theta,\varphi)\cdot\mathbf{e_1}(\varphi) \tag{2a}$$

$$f_2(\theta,\varphi) = \mathbf{E}_S(\theta,\varphi)\cdot\mathbf{e_2^i}(\varphi)\,, \tag{2b}$$

where $\mathbf{E_S}(\theta,\varphi) = (E_{Sx}, E_{Sy}, 0)$ is the input beam considered transverse and the dot stands for the inner product. Vectors $\mathbf{e_1}$ and $\mathbf{e_2^i}$ are unit vectors in the radial and azimuthal directions whereas $\mathbf{e_2^o}$ is the projection of $\mathbf{e_2^i}$ on the convergent wavefront surface, as shown in Fig. 1. This figure shows the geometrical variables used throughout this paper at different reference surfaces. Vectors $\mathbf{e_1}$, $\mathbf{e_2^i}$ and $\mathbf{e_2^o}$ are given by

$$\mathbf{e_1}(\varphi) = (-\sin\varphi, \cos\varphi, 0) \tag{3a}$$

$$\mathbf{e_2^i}(\varphi) = (\cos\varphi, \sin\varphi, 0) \tag{3b}$$

$$\mathbf{e_2^o}(\theta,\varphi) = (\cos\theta\cos\varphi, \cos\theta\sin\varphi, \sin\theta)\,. \tag{3c}$$

To analyze the polarization structure of $\mathbf{E}(r,\phi,z)$, an alternative base of mutually perpendicular unit vectors $\mathbf{u}_+$, $\mathbf{u}_-$ and $\mathbf{u_z}$ is used

$$\mathbf{u}_\pm = \frac{1}{\sqrt{2}}(1,\pm i,0) \quad \mathbf{u_z} = (0,0,1)\,, \tag{4}$$

#205396 - $15.00 USD Received 23 Jan 2014; revised 4 Mar 2014; accepted 5 Mar 2014; published 17 Mar 2014

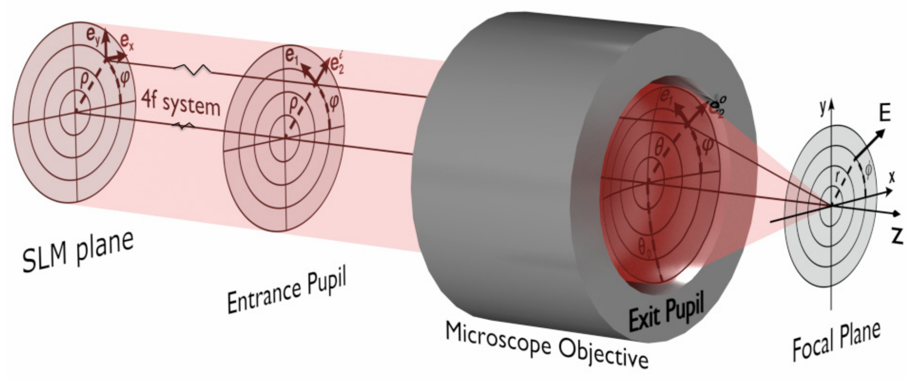

Fig. 1. Notation and sketch of a highly focused optical system.

thus $\mathbf{E}(r,\phi,z) = E_+(r,\phi,z)\,\mathbf{u}_+ + E_-(r,\phi,z)\,\mathbf{u}_- + E_z(r,\phi,z)\,\mathbf{u_z}$. According to Eq. (1), components (E_+, E_-, E_z) read

$$E_\pm(r,\phi,z) = \frac{A}{\sqrt{2}}\int_0^{\theta_0}\int_0^{2\pi}\sqrt{\cos\theta}\left[\mp i f_1(\theta,\varphi) + \cos\theta\, f_2(\theta,\varphi)\right]\times \\ \times e^{ikr\sin\theta\,\cos(\phi-\varphi)}e^{-ikz\cos\theta}e^{\mp i\varphi}\sin\theta\, d\theta\, d\varphi \tag{5a}$$

$$E_z(r,\phi,z) = A\int_0^{\theta_0}\int_0^{2\pi}\sqrt{\cos\theta}\sin\theta\, f_2(\theta,\varphi)\, e^{ikr\sin\theta\,\cos(\phi-\varphi)}e^{-ikz\cos\theta}\sin\theta\, d\theta\, d\varphi\, . \tag{5b}$$

Notice that $E_\pm$ represent the right (+) and left (-) circular content of the transverse field at the vicinity of the focus plane and E_z is the magnitude of the longitudinal component. Since our goal is to generate a focused field whose transverse component is circularly polarized at any plane z, either E_+ or E_- has to be zero. This condition is fulfilled when $f_1(\theta,\varphi) = \pm i\cos\theta\, f_2(\theta,\varphi)$, which is equivalent to

$$f_1(\theta,\varphi) = \pm\, i\cos\theta\, g(\theta,\varphi) \tag{6a}$$
$$f_2(\theta,\varphi) = g(\theta,\varphi) \tag{6b}$$

where, $g(\theta,\varphi)$ is an arbitrary function. Additional characteristics of the global field can be obtained by choosing a suitable function $g(\theta,\varphi)$. For example, to obtain a non-zero longitudinal component at the axis implies that $g(\theta,\varphi) = g(\theta)$.

In what follows and without loss of generality we choose the plus sign, i.e. we deal with right handed circularly polarized fields. For this kind of incident beams the transverse and longitudinal components of $\mathbf{E}(r,\phi,z)$ become

$$E_+(r,\phi,z) = \frac{2A}{\sqrt{2}}\int_0^{\theta_0}\int_0^{2\pi}\sqrt{\cos\theta}\cos\theta g(\theta)e^{-i\varphi}e^{ik\sin\theta r\cos(\phi-\varphi)}e^{-ikz\cos\theta}\sin\theta d\theta d\varphi \tag{7a}$$
$$E_-(r,\phi,z) = 0 \tag{7b}$$
$$E_z(r,\phi,z) = A\int_0^{\theta_0}\int_0^{2\pi}\sqrt{\cos\theta}\sin\theta g(\theta)e^{ik\sin\theta r\cos(\phi-\varphi)}e^{-ikz\cos\theta}\sin\theta d\theta d\varphi\, . \tag{7c}$$

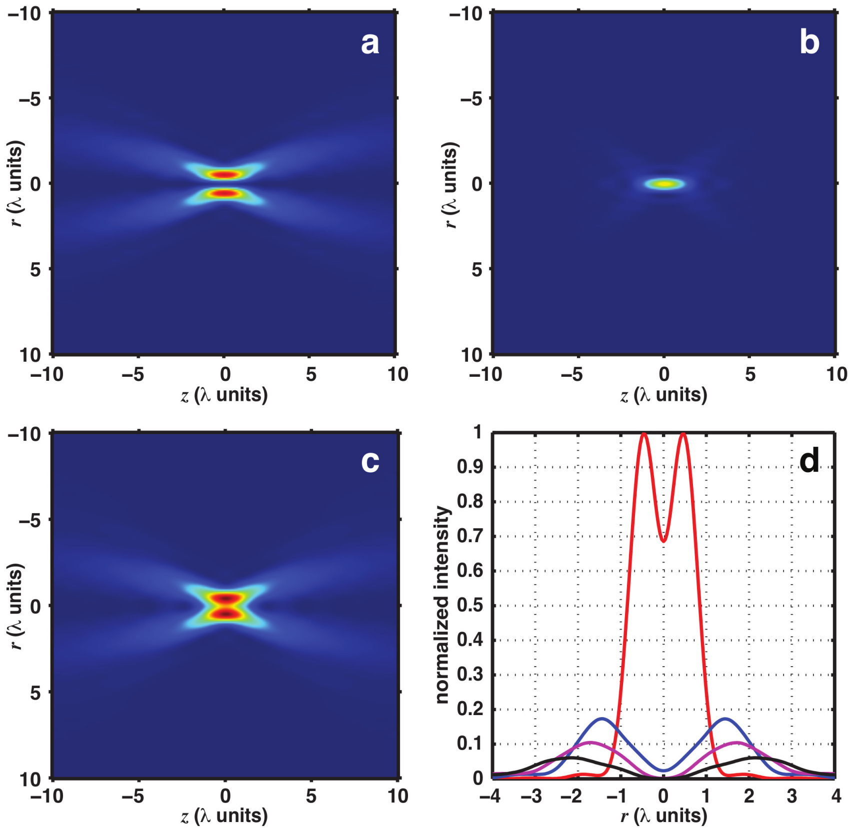

Fig. 2. Irradiance maps for a circularly-polarized highly-focused beam ($NA = 0.85$): (a) $|E_+|^2$, (b) $|E_z|^2$ and (c) I. (d) Profiles of I at $z = 0$ (red) $z = -3\lambda$ (blue), $z = -5\lambda$ (magenta) and $z = -7\lambda$ (black).

Integrating over φ, field components E_+ and E_z take the form

$$E_+(r,\phi,z) = i\frac{4\pi A}{\sqrt{2}}e^{-i\phi}\int_0^{\theta_0}\sqrt{\cos\theta}\cos\theta\, g(\theta)\, J_1(kr\sin\theta)\, e^{-ikz\cos\theta}\sin\theta\, d\theta \tag{8a}$$

$$E_z(r,z) = 2\pi A\int_0^{\theta_0}\sqrt{\cos\theta}\sin\theta g(\theta)\, J_0(kr\sin\theta)\, e^{-ikz\cos\theta}\sin\theta d\theta\ , \tag{8b}$$

where $J_0(x)$ and $J_1(x)$ are the first kind Bessel functions of order 0 and 1 respectively. Interestingly, E_+ presents topological charge $e^{-i\phi}$ and $|E_+|^2$ and $|E_z|^2$ show circular symmetry.

Figure 2 show irradiance maps for (a) the transverse component $|E_+|^2$, (b) the longitudinal component $|E_z|^2$ and (c) the total field $I = |E_+|^2 + |E_z|^2$ when a microscope objective $NA = 0.85$ ($\theta_0 \approx 1$ rad) is used. The illumination is assumed to be Gaussian i.e. $g(\theta) = \exp\left(-\frac{1}{f_0}\frac{\sin\theta}{\sin\theta_0}\right)^2$ and the filling factor f_0 is set to 1. Notice that $|E_z|^2$ presents high values at $z = 0$ and drops very fast out of the focal plane. On the other hand, $|E_+|^2 = 0$ at $r = 0$ at any plane z. Figure 2(d) shows the profiles of the total irradiance I at different distances from the focal plane ($z = 0$, $z = -3\lambda$, $z = -5\lambda$ and $z = -7\lambda$).

#205396 - $15.00 USD Received 23 Jan 2014; revised 4 Mar 2014; accepted 5 Mar 2014; published 17 Mar 2014

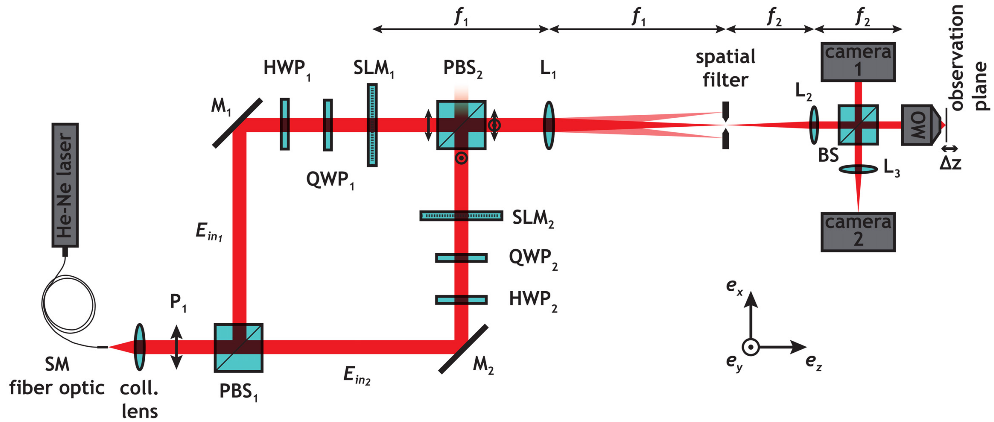

Fig. 3. Sketch of the optical setup. Light source: HeNe laser $\lambda = 633\,nm$; P_1, P_2 and P_3: linear polarizers; PBS_1 and PBS_2; polarizing beam splitters; M_1 and M_2: mirrors; HWP: half-wave plate: QWP: quarter-wave plate; SLM_1 and SLM_2: spatial light modulators; L_1, L_2 and L_3: lenses; BS: beam splitter; MO: microscope objective.

3. Synthesis of beam $\mathbf{E}_S$

Figure 3 depicts an experimental setup based on a Mach-Zehnder interferometer able to generate arbitrary spatially-variant polarized focused beams. An extended explanation on how this procedure can be used to generate beams with arbitrary polarization and shape can be found in [17]. A linearly polarized input beam $\mathbf{E}_{in}$ is split into two beams by means of polarizing beam splitter PBS_1. Reflected by mirrors M_1 or M_2 the split beam (E_{in1} or E_{in2}) passes through wave plates HWP and QWP which rotate the oscillating plane and set the modulator to the required desired modulation curve. Then, light passes through a translucent SLM (Holoeye HEO 0017) displaying cell-based double-pixel holograms to encode complex transmittances $C_x(x,y)$ and $C_y(x,y)$ [34].

Precise alignment of the different optical components is required, especially a good match between the corresponding pixels of the two SLMs. This is carried out during the set up procedure by displaying the same distribution on SLM_1 and SLM_2 and imaging these scenes on camera 1. Note that both displays are controlled independently. Then, the scene displayed on one of the screens is shifted until a perfect match with the other one is accomplished. Shift values are used later to adapt the holograms displayed on both SLMs.

These beams are subsequently recombined by means of polarizing beam splitter PBS_2 and fed into a *4f* system. A spatial filter removes higher-order terms whereas allowing pass the synthesized field $\mathbf{E}_S$. The irradiance of this beam can be observed by means of camera 1. Afterward, $\mathbf{E}_S$ is focused by means of a high numerical aperture microscope objective (MO) $NA = 0.85$. The beam in the focal area is reflected on a glass surface and imaged on camera 2. Polarization analysis is carried out by placing a polarizer (and a quarter-wave plate if required) next to camera 2.

According to Eqs. (2) and (6), the synthesized beam $\mathbf{E}_S$ has to be

$$\mathbf{E_S} = (\cos\varphi - i\cos\theta\sin\varphi)\, g(\theta)\,\mathbf{e_x} + (\sin\varphi + i\cos\theta\cos\varphi)\, g(\theta)\,\mathbf{e_y} \tag{9}$$

where $\mathbf{e_x}$ and $\mathbf{e_y}$ are orthogonal Cartesian unit vectors as shown in Fig. 1. In order to synthesize

#205396 - $15.00 USD Received 23 Jan 2014; revised 4 Mar 2014; accepted 5 Mar 2014; published 17 Mar 2014

$\mathbf{E_S}$ the following complex valued distributions are coded on each SLM

$$C_x(\rho,\varphi) = \cos\varphi - i\sqrt{1-\rho^2}\sin\varphi \tag{10a}$$

$$C_y(\rho,\varphi) = \sin\varphi + i\sqrt{1-\rho^2}\cos\varphi\,. \tag{10b}$$

It is assumed that the radius of the entrance pupil is set to 1 and $\rho = \sin\theta$ is the radial distance from the optical axis at the entrance pupil plane (see Fig. 1).

Figure 4 is a polar diagram displaying the values of the complex plane accessible by the codification method (gray small dots) and the set of physically accessible values by modulator SLM_1 (red dots). A certain value C can be accessed as a combination of phasors M_L and M_R, that belong to the modulation curve, and E_L and E_R, that are diffracted off-axis and removed by the spatial filter at the focal plane of lens L_1. As shown in this Figure, not all values of the complex plane are accessed by the encoding procedure. This drawback could be overcome using a light source with a shorter wavelength to improve the modulation response of the SLM [35]. However, if the subset of accessible values C within the circle of transmittance $T = 0.3$ is used (see inset in Fig. 4), almost any complex transmittance can be generated. Non accessible values are approximated to the closest one belonging to the subset.

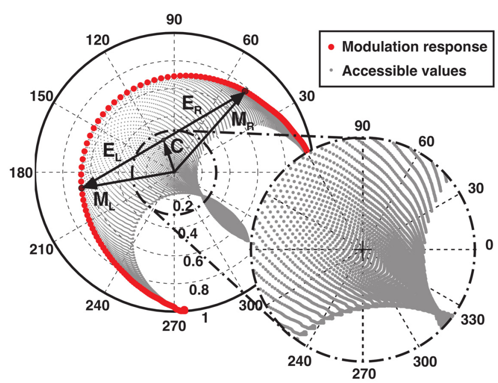

Fig. 4. A certain complex value C is generated as a combination of phasors M_L and M_R (that belong to the modulation response curve), and E_L and E_R that are diffracted off-axis and removed. The inset shows the subset of C values used to generate the holograms.

4. Experimental results

As explained in the previous section, the synthesized beam $\mathbf{E_S}$ is focused by means of the objective lens and subsequently reflected on the cover slip, back-propagated through the objective and imaged on camera 2 aided by lens L_2. The cover slip (observation plane) is mounted on a stage that enables to modify the observation distance z. Figure 5 (first row) shows the irradiance I at $z = -3.5\lambda$, -5λ and -7λ. Distance z is estimated by comparing the angular average of the experimental images with the numerical evaluation of I and $|E_+|^2$ (Eqs. (8a) and (8b)). These curves are presented in the second row of Fig. 5. Notice that the irradiance at the focal plane $z = 0$ is not analyzed due to lack of accuracy along the z-axis and insufficient resolution of the camera. Furthermore, the sudden increase in irradiance around the focal plane complicates the analysis, because camera is saturated.

To analyze the polarization of the focused beam a measure of the Stokes parameters has been

 Received 23 Jan 2014; revised 4 Mar 2014; accepted 5 Mar 2014; published 17 Mar 2014

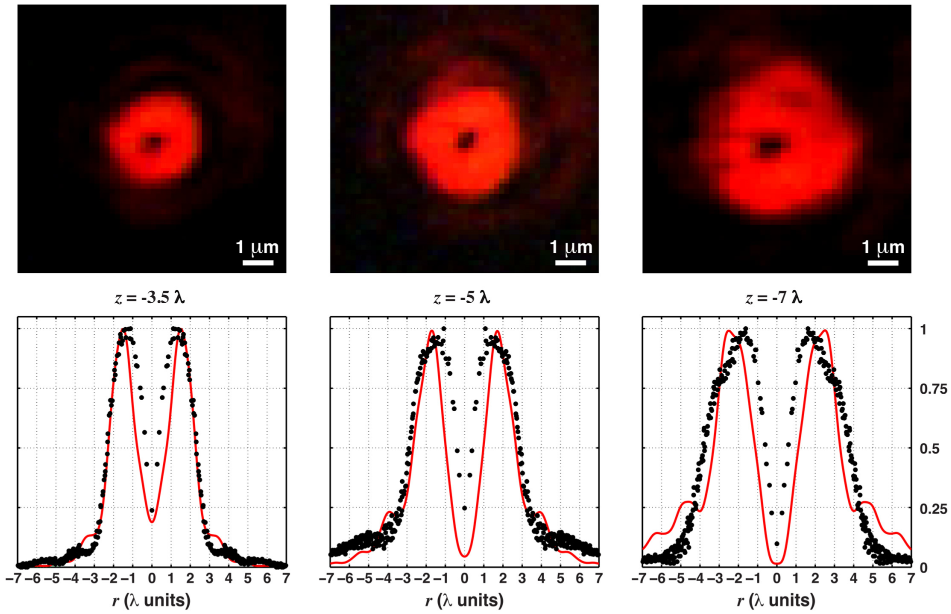

Fig. 5. Experimental results at the observation plane: the first row corresponds to the image captured by camera 2. These images are normalized to its corresponding maximum. The second row shows the profile of the experimental images (black dots) and the numeric evaluation of I(red solid line) for $z = -3.5\lambda$, -5λ and -7λ.

carried out. These parameters are obtained according to

$$S_0 = I(0^\circ,0)+I(90^\circ,0) \tag{11a}$$
$$S_1 = I(0^\circ,0)-I(90^\circ,0) \tag{11b}$$
$$S_2 = I(45^\circ,0)-I(135^\circ,0) \tag{11c}$$
$$S_3 = I(45^\circ,\pi/2)-I(135^\circ,\pi/2)\ , \tag{11d}$$

where $I(\alpha,\beta)$ stands for the recorded intensity when a polarizer is set at an angle α with respect to the x direction in front of camera 2; β is the retardation between the x and y directions [36]. Retardation $\beta = \pi/2$ is accomplished by using also a quarter wave plate. Once the Stokes parameters are found in each point of the beam, the polarization map can be generated. Figure 6 show the Stokes images S_0, S_1, S_2, S_3 for the focused field at $z = -3.5\lambda$. Notice that the values of images S_1 and S_2 are very close to zero, whereas the high values present in S_3 demonstrates that the field is circularly polarized.

In order to provide global parameters to describe the polarization of the whole beam, the following cumulative values S_i are introduced:

$$\mathsf{S}_i^2 = \frac{\sum S_i^2(k,l)}{\sum S_0^2(k,l)} \qquad \mathrm{i} = 1,2,3 \tag{12}$$

where (k,l) are the indexes of the pixels of the Stokes image. Table 4 shows the values of S_1, S_2, S_3 for the three positions of the observation plane considered. A clear circular character of the beam along the z-axis is recognized since $\mathsf{S}_3^2 \gg \mathsf{S}_1^2 + \mathsf{S}_2^2$ at any transverse plane z.

#205396 - $15.00 USD Received 23 Jan 2014; revised 4 Mar 2014; accepted 5 Mar 2014; published 17 Mar 2014

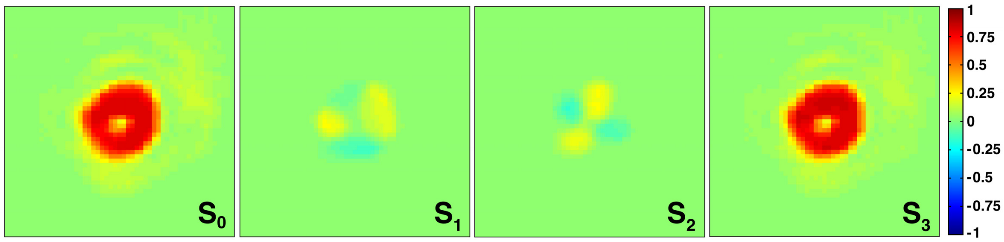

Fig. 6. Stokes images of the focused field at $z = -3.5\lambda$.

Table 1. S_i values for the three transverse planes z analyzed.

z	S_1	S_2	S_3
-3.5λ	0.053	0.044	0.965
-5λ	0.051	0.045	0.966
-7λ	0.052	0.047	0.967

5. Conclusions

In this paper, a method for generating highly focused beams with circular polarization at any plane is presented. Using the Richards-Wolf diffraction formalism analytical expressions have been developed to design such fields. The analysis of the field in the focal area shows that the irradiance of the longitudinal component present very high values. The use of an interferometric setup for generating beams with arbitrary polarization combined with the use of digital holography techniques has enabled the experimental generation of such beams. Satisfactory practical results have been obtained showing a good agreement between theoretical predictions and the experimental behavior of the beam.

Acknowledgment

This work was funded in part by the Spanish Ministerio de Ciencia e Innovación, project FIS2010-17543.